TOWARDS EXPERIMENTALLY-INFORMED MODELING OF CONDUCTION FOR IMPROVED FINITE ELEMENT THERMAL PREDICTION OF WIRE-ARC DIRECTED ENERGY DEPOSITION

Ally Cummings[1,2], Walker Jarrell[1], Matthew W. Priddy[1,2]

[1]Center for Advanced Vehicular Systems, Mississippi State University
[2]Michael W. Hall School of Mechanical Engineering, Mississippi State University

Abstract

Wire-arc directed energy deposition (arc-DED) is a metal-based additive manufacturing process known for its high deposition rates, which enable the production of medium to large-scale components. Due to the cyclic heating and cooling associated with this process, resultant parts experience residual stress and distortion. Finite element (FE) simulations can be used to predict the thermomechanical response of arc-DED parts. FE thermal models have previously only consisted of the part and substrate to minimize computational time. A shortcoming of this approach is the inability to capture conduction that is experimentally known to occur through the print assembly. As a result, the convection boundary conditions are artificially elevated to produce results that match experimental data. This work explores a more informed modeling approach that includes fixturing components to accurately simulate conduction through the assembly. This model offers potential for improved predictions and increased repeatability across different parts by reducing model calibration requirements.

Introduction

Wire-arc directed energy deposition (arc-DED) is a metal-based additive manufacturing (AM) process that uses a wire feedstock and an electric arc heat source to deposit material in a layer-by-layer welding manner [1]. The many potential advantages of arc-DED are propelling industry interest in this technology. These advantages include the ability to produce large-scale parts due to its high deposition rates, reduced material waste, and relatively low investment costs compared to other AM technologies [2], [3], [4], [5], [6]. Despite the benefits of arc-DED as a manufacturing solution, several problems still need to be addressed. Defects are often observed in arc-DED parts that can prevent them from being usable. A primary issue that needs to be resolved is the high residual stress in the parts resulting from the cyclic heating and cooling inherent to the deposition process [7], [8], [9], [10]. This residual stress causes distortion, and it can compromise the mechanical integrity of the final part [10], [11]. Moreover, porosity and geometric issues with the deposited beads commonly occur when incorrect parameter sets are chosen [12]. Research efforts are being made to optimize arc-DED so that it can become a widespread manufacturing option for certain components. One method for studying arc-DED is finite element (FE) modeling. FE modeling of arc-DED is an efficient tool for predicting the thermal and mechanical response of parts being printed [1], [13], which is advantageous for the development and understanding of this technology.

When printing, the part is deposited onto a substrate plate which is fastened to the worktop by various fixturing components. This is necessary to secure the specimen during printing and prevent geometric issues as the part begins to warp [14]. These accessory components are referred

to as the print assembly. It is experimentally known that conduction between various components of the print assembly can contribute significantly to the thermal response of the part. However, FE thermal models for arc-DED typically only consist of the part and substrate to minimize computational time [5], [15]. As a result, heat transfer boundary conditions must be manipulated to account for the conduction occurring through the print assembly. This is often done by increasing the convection term [7], [9], [16]. The applied convection boundary conditions are determined during a time-consuming calibration process which involves adjusting the heat transfer coefficients to produce simulation results that match the experimental data [17], [18]. While this can result in accurate thermal predictions, it is not a robust method because the boundary conditions are not physically-motivated. Rather, the calibrated convection terms are artificially high to account for conduction, which varies across different prints and assemblies. Therefore, these terms must be recalibrated for every print, hindering the predictive capabilities of the models.

To reduce assumptions in the analysis, there is motivation to model the assembly to produce more informed thermal predictions despite the increase in computational cost. By including the assembly components, conduction can be represented in the model, and justifiable convection boundary conditions can be applied. Furthermore, it is hypothesized that calibrated assembly models will provide accurate thermal predictions across different parts, which would greatly advance FE modeling as a predictive tool for arc-DED. Because residual stress and distortion are thermally-driven, the improved temperature histories, which are the primary boundary condition for mechanical models [19], should likewise improve mechanical predictions.

The overarching goal of this study is to demonstrate improved FE thermal predictions for arc-DED parts by using models that include the assembly components. Conductive heat transfer through the assembly will be simulated to improve the convection boundary conditions and increase the overall model fidelity. Four parts of varying geometry and size will be printed using a consistent print assembly setup. An assembly model will be calibrated to one part, and the calibrated boundary conditions will subsequently be applied to the remaining parts. Experimental data comparisons will be made to assess the accuracy of assembly models for various prints. Conclusions will be drawn regarding the potential benefits and improvements of assembly models compared to traditional part and substrate models. Overall, this work aims to contribute to the refinement of FE modeling for thermomechanical prediction of arc-DED for the advancement of this technology.

Methodology

Experimental Methods

Three 1" components – a thin wall, S wall, and cylinder (*Figure 1*) – and a 5" thin wall (*Figure 3*) were selected for this study. These parts were chosen to provide variation in both geometry and size for the purpose of evaluating the accuracy of assembly models across different parts. The print material was ER120S-G, which was deposited onto A36 mild steel substrates. All parts were printed using a Fronius TPS-400i Cold Metal Transfer (CMT) welding source.

1" Geometries

The 1" tall parts were comprised of 15-layers deposited onto 6" x 3" x 0.5" substrates (*Figure 1*). The wire feed speed and travel speed were 200 ipm and 8 mm/s, respectively. The

resulting bead shape using these parameters was approximately 7.0 mm wide and 1.75 mm high. All three parts were printed with an alternating direction toolpath where the end point for one layer became the start point for the next layer. A fixed dwell time of 180 seconds was chosen for the part to partially cool between each layer. During the cylinder print only, a technological issue occurred after the first layer, so there was an extended dwell period of 665 seconds at that single instance. It was not necessary to reprint the part because the delay can be implemented in the model and does not affect the integrity of the study. Thermal data was collected using five K-type thermocouples (TCs) welded onto the substrate for each print. A TC was attached at the center of each of the four vertical faces of the substrate, and one additional TC was attached at the center of the bottom face of the substrate (*Figure 2*). A 25 Hz sampling rate was used to record TC measurements.
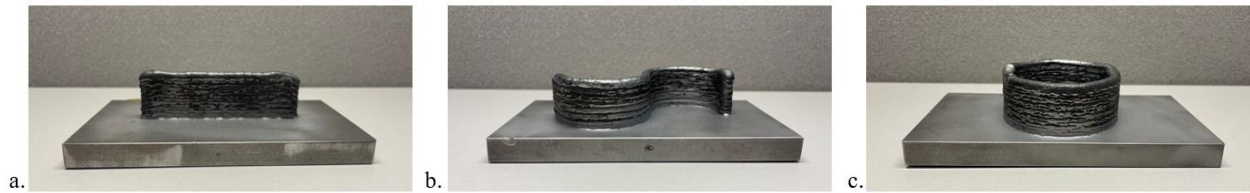

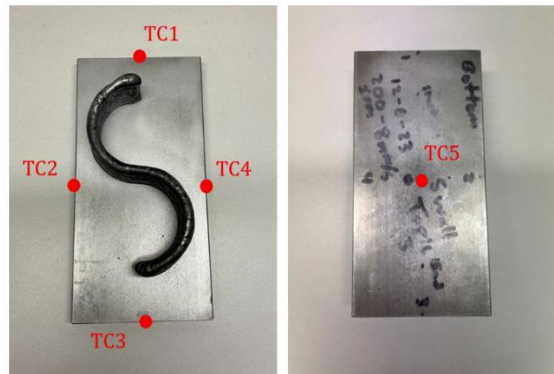*Figure 1. The 1" a) thin wall, b) S wall, and c) cylinder parts.*

Figure 2. Locations of the K-type thermocouples used to collect thermal data on the substrate of the 1" prints.

5" Thin Wall

The 5" thin wall was printed on a 12" x 3" x 0.5" substrate (*Figure 3*). The wire feed speed was 200 ipm, and the travel speed was 4 mm/s. The dimensions of the resultant part were 254 x 10.5 x 127 mm. An alternating direction toolpath was used to deposit the 64-layers of material, and a 152 s dwell time was implemented between each layer. Data from three K-type TCs welded onto the vertical faces of the substrate was collected (*Figure 3*). TC data was logged at a 5 Hz sampling rate.
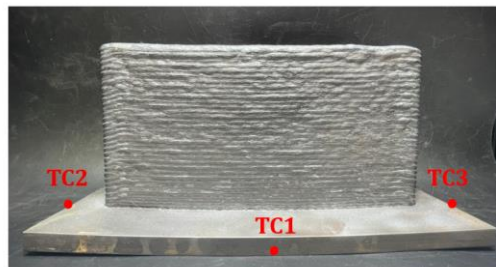

Figure 3. The 5" thin wall and the locations of 3 K-type thermocouples used to collect thermal data on the substrate.

Print Assembly

The print assembly remained constant and consisted of a 0.5 x 0.5 m 5050 Aluminum T-slot plate and 4 A36 toe clamps that were 2.5" in length. The clamps were applied at the corners of the substrate as shown in *Figure 4*. All clamps were torqued to 30 ft·lb to ensure uniform fixturing.

Finite Element Modeling

Experimental dimensions were used to generate computer aided drawing (CAD) models for the parts. The CAD models for the clamps and T-slot plate were simplified into rectangular geometries for ease of meshing. The goal of modeling the assembly is to represent conductive heat transfer resulting from fixturing more accurately in the system; therefore, the most important aspect of these geometries was the mass which draws heat from the system. The models were then assembled and discretized into a FE mesh using Abaqus/CAE 2022. *Figure 4* depicts the FE mesh assigned to the parts, and the mesh details are presented in *Tables 1-2*. The 1" thin wall, S wall, cylinder, and 5" thin wall models have 263,170, 414,402, 396,970, and 359,702 elements, respectively. Including the clamps and T-slot plate only posed an increase of 2,562 elements compared to the part and substrate only. Linear hexahedral heat transfer elements (DC3D8) were used for all simulations. The elements on the 1" parts had a seed size of 0.5 mm to provide a fine mesh where the data is of primary interest. Due to its substantial increase in size, the 5" thin wall was meshed with 1 mm elements. Likewise, the assembly components were meshed coarsely to reduce the overall computational cost. The average aspect ratio for each meshed component is presented in *Table 2*. Surface-to-surface tie constraints were applied to all contacting components. No significant warping was observed during experimentation, nor did any clamps fail. Therefore, the assumption was made that all points of contact were maintained throughout deposition.
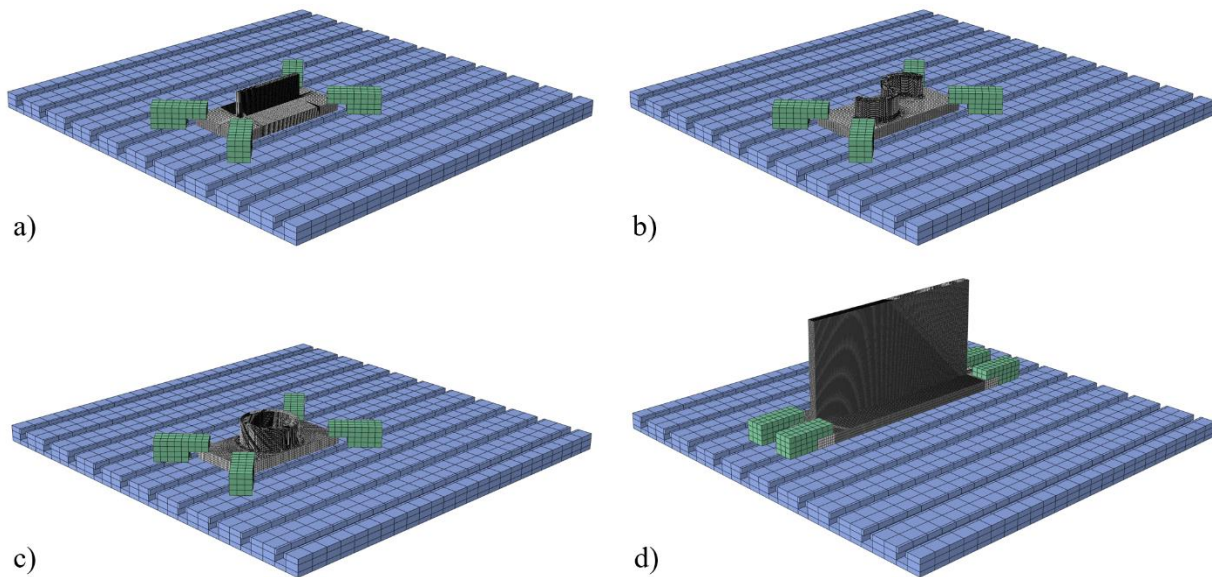

a)

b)

c)

d)

Figure 4. FE mesh generated for the a) 1" thin wall, b) S wall, c) cylinder, and d) 5" thin wall models.

Table 1. Number of elements and nodes in the FE mesh for the part and substrate only compared to the entire model.

Geometry	Part and Substrate		Entire Model	
	# Elements	# Nodes	# Elements	# Nodes
1" Thin Wall	260,608	284,127	263,170	289,015
S Wall	411,840	440,824	414,402	445,712
Cylinder	394,408	431,252	396,970	436,140
5" Thin Wall	357,140	400,950	359,702	405,838

Table 2. Average aspect ratio of the mesh generated for each component.

Component	1" Thin Wall	S Wall	Cylinder	5" Thin Wall	T-slot	Clamp
Average Aspect Ratio	1.01	1.30	1.13	1.20	3.93	1.31

Temperature-dependent thermophysical properties for ER120S-G were generated in JMatPro software using the composition detailed in *Table 3*. Density, thermal conductivity, and specific heat properties for all materials were input into the simulations. The input density values for ER120S-G, A36, and Aluminum were 7.83 $\frac{g}{cm^3}$, 7.85 $\frac{g}{cm^3}$ [20], and 1.0 $\frac{g}{cm^3}$ [21], respectively. The temperature-varying thermal conductivity and specific heat values used for ER120S-G and A36 are displayed in *Figure 5*. Specific heat values for ER120S-G were linearized to avoid model convergence errors. The properties for Aluminum were constant values of 105 $\frac{W}{m^2\,°C}$ for thermal conductivity and 897 $\frac{J}{kg\,°C}$ for specific heat [21].

Table 3. Material composition for ER120S-G used to generate thermophysical properties in JMatPro.

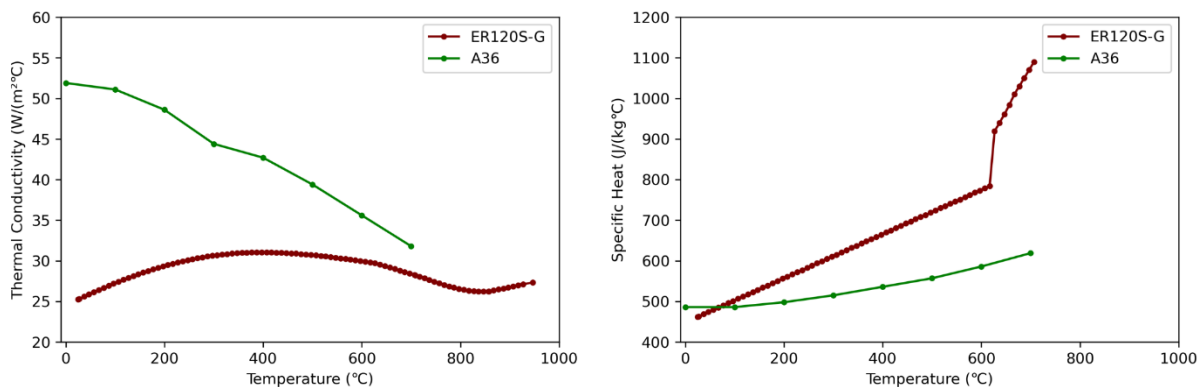| Element	Fe	Al	Cr	Cu	Mn	Mo	Ni	Si	Ti	V	C	P	S
Wt. %	93.323	0.004837	0.326	0.148	1.871	0.946	2.262	0.403	0.687	0.003653	0.01938	0.002777	0.002874

Figure 5. Temperature-dependent thermal conductivity and specific heat values for ER120S-G and A36 [20].

The Goldak heat source (*Figure 6*) was used in all simulations. Goldak is a higher fidelity numerical model that has been used widely for simulating welding processes including arc-DED

because its shape closely resembles the observable melt pool [22], [23], [24]. The following equations define the heat flux for Goldak's model:

$$q_f(x,y,z) = \frac{6\sqrt{3}f_f Q}{bca_f\pi\sqrt{\pi}} \cdot e^{-3\frac{x^2}{a_f^2}} \cdot e^{-3\frac{y^2}{b^2}} \cdot e^{-3\frac{z^2}{c^2}} \qquad (1)$$

$$q_r(x,y,z) = \frac{6\sqrt{3}f_r Q}{bca_r\pi\sqrt{\pi}} \cdot e^{-3\frac{x^2}{a_r^2}} \cdot e^{-3\frac{y^2}{b^2}} \cdot e^{-3\frac{z^2}{c^2}} \qquad (2)$$
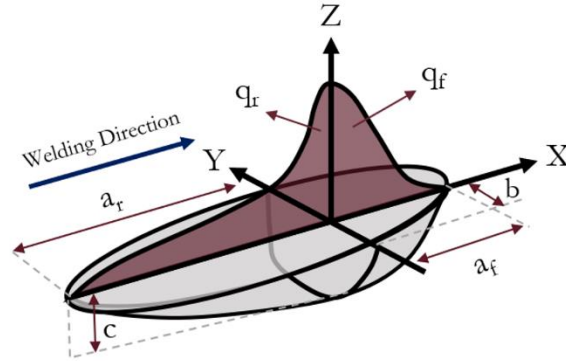

Figure 6. Goldak double ellipsoid model for a moving heat source (reproduced from [22]).

Eight parameters are used to define the Goldak heat source. *Table 4* shows the heat source parameters chosen for these analyses, which were adapted from literature [5], [25]. The spot radius, b, was calculated as half the experimental bead width, which was 3.5 mm for the 1" parts and 5.25 mm for the 5" thin wall. The input power for the heat source, Q, was determined by averaging the power values reported by the weld logger while the arc was on. The movement of the heat source was specified using event series that were generated using AMPES [26], a Python script that converts G-code into a time series formatted for Abaqus.

Table 4. Goldak heat source parameters used in the simulations.

Front length	Rear length	Depth	Front fraction	Rear fraction	Efficiency
a_f	a_r	c	f_f	f_r	n
2	6	2.32	0.5	1.5	0.95

All nodes were given an initial temperature of 300 K. Convection and radiation boundary conditions were defined. Compared to conduction and convection, heat loss due to radiation is minimal [16], so an emissivity value of 0.01 was applied. Because literature currently lacks a clear method for specifying convection in arc-DED models, an average coefficient of convection, h, was applied to all exterior elements. The value of h was determined by calibrating the 1" thin wall simulation to experimental thermocouple data, which is the common mode for determining heat transfer coefficients in literature [7], [17]. While more robust boundary conditions are preferred, the calibrated h value in this model intends to account solely for convection, an improvement from previous models. To calibrate the convection, the 1" thin wall simulation was initially run using $18\frac{W}{m^2K}$ [27] for h, which resulted in thermal underprediction. In response, h was decreased to $10\frac{W}{m^2K}$, and good agreement with experimental data was observed. Therefore, $10\frac{W}{m^2K}$ was

selected for the convection boundary condition. Boundary conditions were held constant across all four simulations to evaluate model accuracy without recalibration. Conduction is not defined using boundary conditions, but rather it is accounted for by the input thermal conductivity properties.

Analyses for the three 1" prints were performed in Abaqus/Standard 2022 using 60 CPUs on a Cray CS300-LC cluster with two Intel Xeon Phi CPUs. The 5" thin wall simulation was run in Abaqus/Standard 2023 using 160 CPUs on a Dell PowerEdge C6520 Linux cluster. For computational efficiency, printing steps were run using a 0.5 s time increment, and the cooling steps were run at a 10 s increment.

Results and Discussion

Simulation results were compared with experimental data to evaluate the models. Temperature data was extracted from the nodes that correspond to the TC locations used in the experimental work (*Figures 2-3*). Some TCs failed during deposition, so only the successful data recordings are presented in this paper. The comparisons between simulated and experimental thermal data are shown in the following figures. *Figure 7* displays the results from the 1" thin wall, which were obtained by calibrating the convection boundary condition to align closely with the experimental measurements.
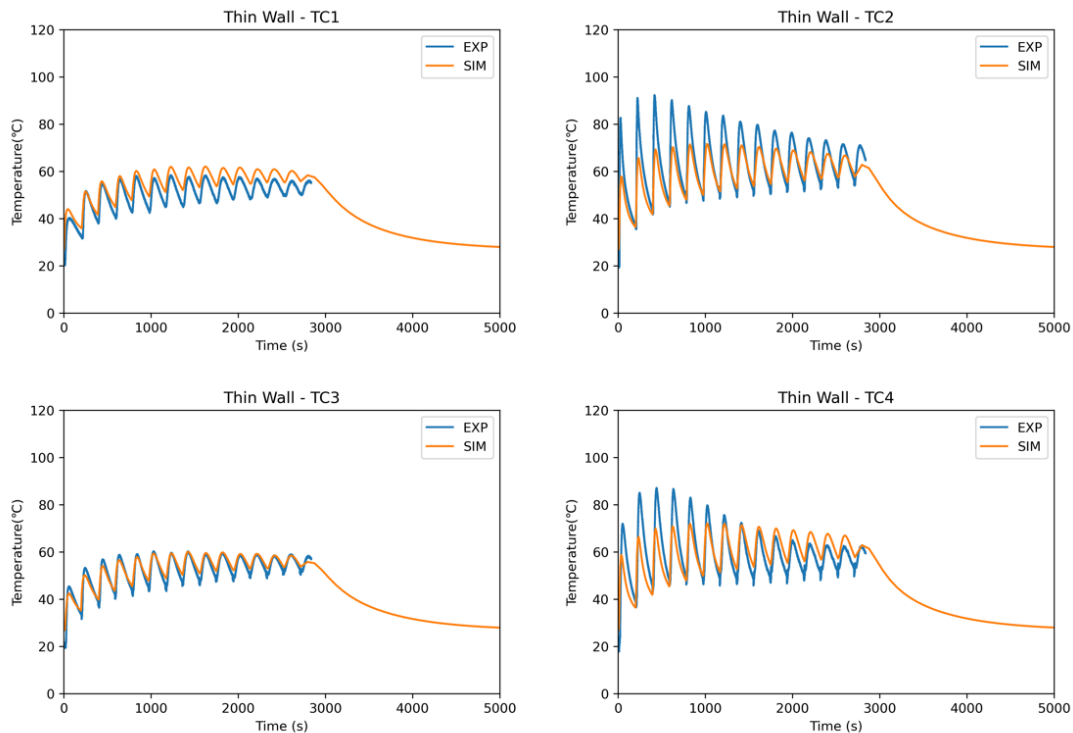

Figure 7. Experimental and simulated thermocouple comparisons for the 1" thin wall part (TC1, TC2, TC3, and TC4).

The calibrated boundary condition was then applied to the S wall, cylinder, and 5" thin wall models, and the TC comparisons for those simulations are presented in *Figures 8-10*. By applying the same boundary conditions and keeping all other model parameters constant, a

determination can be made regarding the improved predictive capabilities of assembly models across parts of different size and shape.
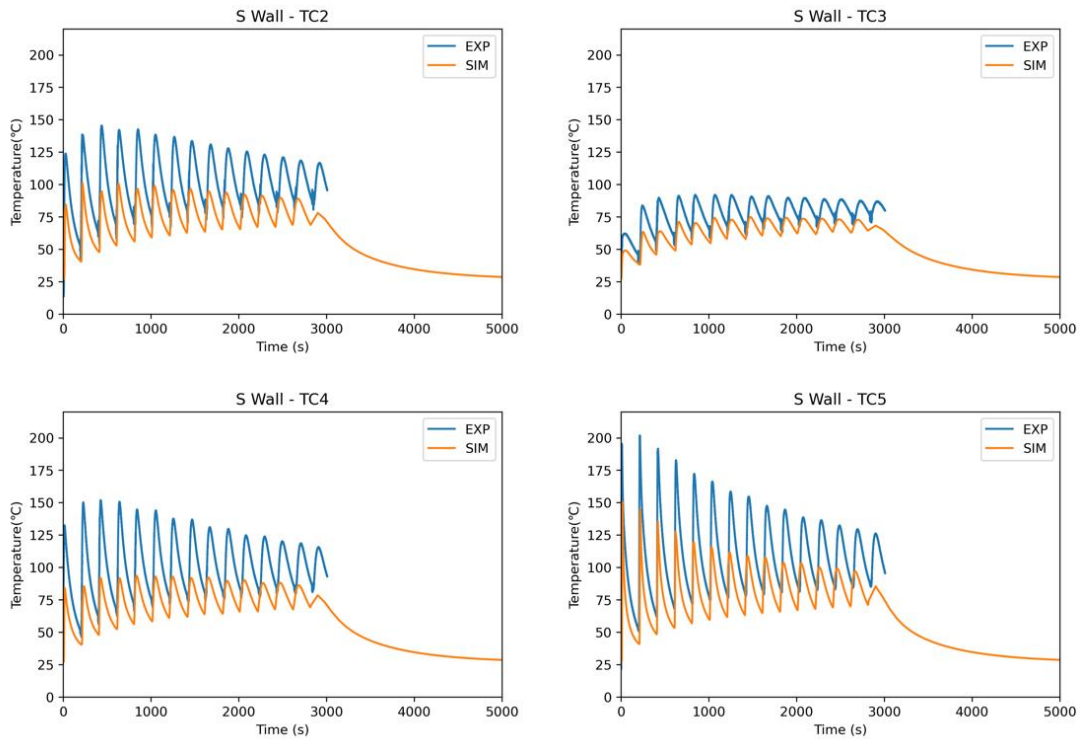

Figure 8. Experimental and simulated thermocouple comparisons for the S wall part (TC2, TC3, TC4, and TC5).
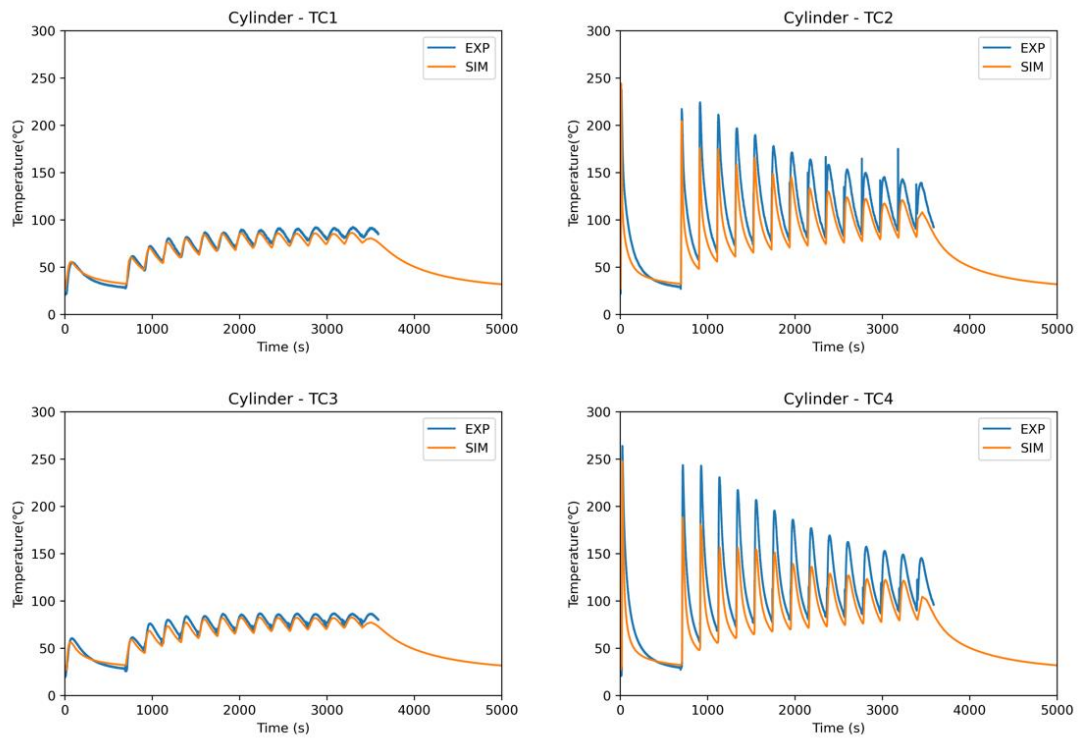

Figure 9. Experimental and simulated thermocouple comparisons for the cylinder part (TC1, TC2, TC3, and TC4).

Overall, the data shows good agreement for the three 1" geometries. By visual inspection, all simulations captured thermal trends through the substrate. The maximum temperatures at the peaks tend to be lower in the simulation compared to the experimental data. This is likely caused by the time increments selected, which may have prevented the simulation from reporting the full thermal profile. Because the heating and cooling rates at the peaks are remarkably high, the time increment would have the most pronounced effect on the results at these points. A finer time increment is expected to demonstrate improved predictions.

Compared to the thin wall and cylinder, the S wall simulation appears to be underpredicting. Although a finer time increment is expected to improve the predictions, it is likely an additional factor is at play. One theory is that the S wall geometry induced a distortion during printing that caused the substrate to separate from the T-slot plate, preventing the part from cooling in the same manner as the other geometries. Conduction from contact with the T-slot plate would draw more heat from the substrate than convection from the air. This would cause the part to have higher experimental temperatures than the simulation, which is what was observed in the results. Though this theory cannot be verified retroactively, it does present a challenge for the modeling approach detailed in this paper. Appropriate clamping techniques should be employed to ensure consistency across different parts using the same assembly configuration so the model can predict accurately. Moreover, this finding should be of interest experimentally because inadequate clamping indeed affects the thermal profile, which may induce heterogeneities in resulting parts.

While the model showed good predictions for the three 1" prints, these parts are highly similar. To further evaluate the repeatability of assembly models, the calibrated model was used to simulate a 5" thin wall. Since conduction is incorporated into assembly models, the convection boundary conditions are expected to be more consistent for larger geometries. Therefore, the 5" thin wall model was prescribed the same boundary conditions. TC comparisons for the 5" thin wall are presented in *Figure 10*.

The results for the 5" thin wall demonstrate logical thermal predictions in the first iteration. The simulation shows instances of underprediction and overprediction, but it matches the general trend well. Similar to the S wall, some of the error is attributed to warping that may have interfered with conduction through the T-slot plate. Since TC2 and TC3 are on opposite sides of a symmetrical print, the thermal history at these locations is anticipated to be nearly identical as predicted by the model. However, the experimental data for TC2 is higher than that of TC3. This, combined with the evident warping of the substrate that can be seen in *Figure 3*, suggests that some of the inaccuracy is a result of contact not being maintained during printing, which is an assumption in the model. Additionally, the boundary conditions in this study are averaged terms determined through calibration. The results show potential for consistent boundary conditions for different prints, but the imprecise average term used in this work does not fully encompass heat transfer for a larger part. Location-specific convection boundary conditions are expected to produce better predictions across parts of different size. Since a principal goal of assembly models is to improve the physical groundings of FE models for arc-DED, future work in this space includes determining robust heat transfer boundary conditions that will increase the accuracy and utility of models.
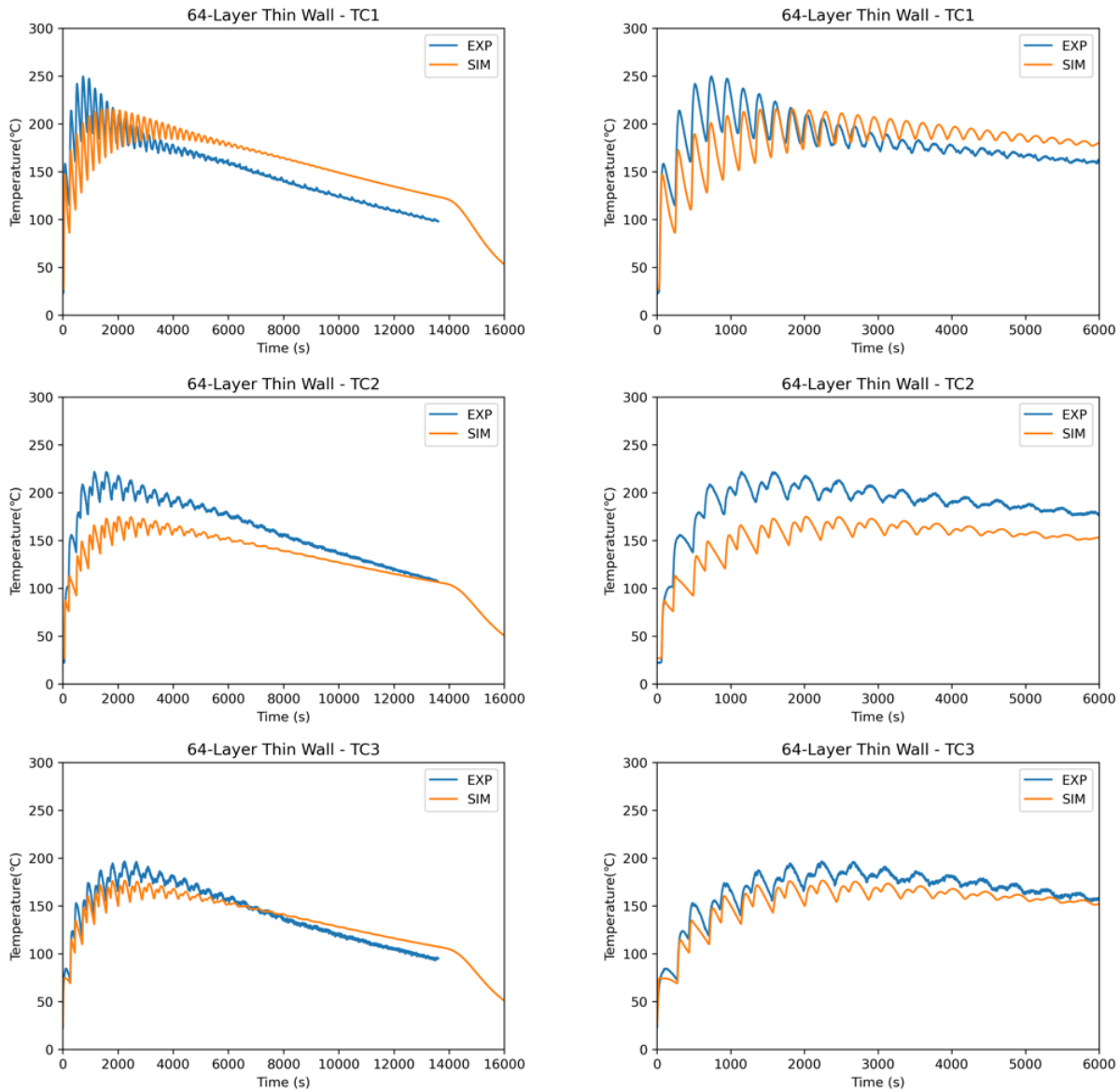
Figure 10. Experimental and simulated thermocouple comparisons for the 5" thin wall (TC1, TC2, and TC3) for the complete time history (left) and the first 6000 s (right).

Despite promising results, an argument against modeling the assembly is the additional computational expense it requires. The increase in number of elements and contact interactions undoubtedly adds computational time. For this work, the three 1" simulations completed in under 4 hours, and the 5" simulation completed within 20 hours. The simulation times were not notably longer than expected based on previous simulation work. However, a precise conclusion cannot be made without running simulations for both modeling approaches using the same computing resources. Future work includes identifying the increase in simulation time assembly models require so the computational limitations of this approach can be established.

Regardless, the minor increase in run time is preferable compared to the numerous iterations necessary to calibrate part and substrate models. To demonstrate this, the 1" thin wall

was also simulated using the part and substrate approach. The model was calibrated in the same manner as the assembly model, beginning with an averaged $18\frac{W}{m^2K}$ for h. It required four iterations to calibrate, and the convection boundary conditions were elevated arbitrarily at locations where conduction was occurring (*Table 5*). The TC comparisons for the part and substrate model and assembly model are displayed in *Figure 11*.

Table 5. Calibrated convection boundary conditions for the part and substrate model for the 1" thin wall.

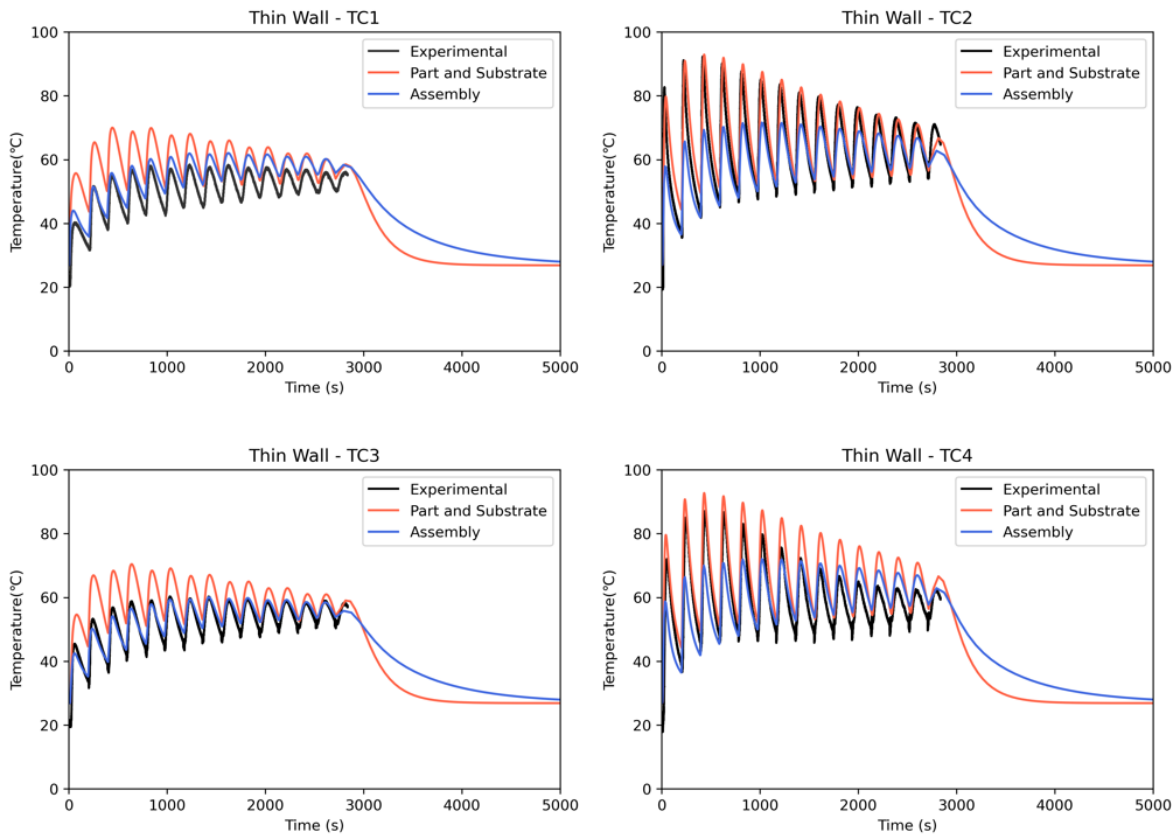| Section	Convection (W/m²K)	Location
Part	18	All elements
Substrate	18	No contact
	100	Contact with clamps
	300	Contact with T-slot

Figure 11. Thermocouple comparisons for the 1" thin wall using a part and substrate model vs. the assembly model.

By comparison, the assembly model is a more efficient modeling approach. The TC results reveal that the two models have approximately the same degree of error, yet the assembly model required 50% less iterations to achieve these results. The inconsiderable increase in run time for assembly models will not exceed the time to run twice as many simulations, so computational expense should not be considered a limitation of assembly models. Furthermore, a reduction in

iterations required to produce accurate predictions is increasingly valuable for large-scale parts with lengthy simulation times. This can be seen in the results for the 5" thin wall. While the model has less accuracy for this large part compared to the 1" geometries, the initial results are significantly closer to being calibrated than if the part and substrate approach was utilized. Therefore, the time it takes to achieve accurate thermal predictions is still reduced by using the assembly model approach even if further calibration is needed. Since this simulation had a run time of approximately 20 hours, the assembly model can potentially save days of computational time to achieve accurate thermal predictions.

Conclusion

FE thermal predictions were made for four arc-DED parts printed using a consistent assembly configuration. The FE models included the assembly components to accurately simulate conduction, which facilitates improved boundary conditions and overall model fidelity. Convection boundary conditions were calibrated for an assembly model and subsequently applied to geometries of varying size or shape. The results demonstrated satisfactory agreement between simulated and experimental data within the first iteration. Inclusion of the assembly components in FE models of arc-DED enables accurate thermal predictions while using a physically-grounded approach. Assembly models offer potential for reduced model calibration time and improved repeatability across different parts. Future work includes refining the heat transfer boundary conditions for the purpose of enhancing accuracy and predictability of models. This work intends to support advancement in FE modeling of arc-DED for the efficient progression of this AM process.

References

[1]   A. Chergui, N. Beraud, F. Vignat, and F. Villeneuve, 'Finite Element Modeling and Validation of Metal Deposition in Wire Arc Additive Manufacturing', in *Lecture Notes in Mechanical Engineering*, Springer Science and Business Media Deutschland GmbH, 2021, pp. 61–66. doi: 10.1007/978-3-030-70566-4_11.

[2]   X. F. Zhao, A. Wimmer, and M. F. Zaeh, 'Experimental and simulative investigation of welding sequences on thermally induced distortions in wire arc additive manufacturing', *Rapid Prototyp J*, vol. 29, no. 11, pp. 53–63, 2023, doi: 10.1108/RPJ-07-2022-0244.

[3]   C. Diao *et al.*, 'WAAM of large-scale space components Manufacture of Large-Scale Space Exploration Components using Wire + Arc Additive Manufacturing'.

[4]   H. Mu, F. He, L. Yuan, P. Commins, H. Wang, and Z. Pan, 'Toward a smart wire arc additive manufacturing system: A review on current developments and a framework of digital twin', Apr. 01, 2023, *Elsevier B.V.* doi: 10.1016/j.jmsy.2023.01.012.

[5]   M. Graf, A. Hälsig, K. Höfer, B. Awiszus, and P. Mayr, 'Thermo-mechanical modelling of wire-arc additive manufacturing (WAAM) of semi-finished products', *Metals (Basel)*, vol. 8, no. 12, Dec. 2018, doi: 10.3390/met8121009.

[6]   V. T. Le, M. C. Bui, T. Q. D. Pham, H. S. Tran, and X. Van Tran, 'Efficient prediction of thermal history in wire and arc additive manufacturing combining machine learning and numerical simulation', *International Journal of Advanced Manufacturing Technology*, vol. 126, no. 9–10, pp. 4651–4663, Jun. 2023, doi: 10.1007/s00170-023-11473-3.

[7]   A. Bauer, R. Scharf, A. Hälsig, and B. Awiszus, 'Numerical simulation and calibration of a single seam WAAM process with a commercial and an open source software', *Journal*

of Applied Engineering Design and Simulation, vol. 1, no. 1, Oct. 2021, doi: 10.24191/jaeds.v1i1.21.

[8]   E. Aldalur, F. Veiga, A. Suárez, J. Bilbao, and A. Lamikiz, 'High deposition wire arc additive manufacturing of mild steel: Strategies and heat input effect on microstructure and mechanical properties', *J Manuf Process*, vol. 58, pp. 615–626, Oct. 2020, doi: 10.1016/j.jmapro.2020.08.060.

[9]   K. P. Prajadhiana *et al.*, 'Experimental verification of computational and sensitivity analysis on substrate deformation and plastic strain induced by hollow thin-walled WAAM structure', *Rapid Prototyp J*, vol. 28, no. 3, pp. 559–572, Mar. 2022, doi: 10.1108/RPJ-06-2020-0135.

[10]   H. Huang, N. Ma, J. Chen, Z. Feng, and H. Murakawa, 'Toward large-scale simulation of residual stress and distortion in wire and arc additive manufacturing', *Addit Manuf*, vol. 34, Aug. 2020, doi: 10.1016/j.addma.2020.101248.

[11]   S. Springer *et al.*, 'Chaboche viscoplastic material model for process simulation of additively manufactured Ti-6Al-4 V parts', *Welding in the World*, vol. 67, no. 4, pp. 997–1007, Apr. 2023, doi: 10.1007/s40194-023-01504-8.

[12]   D. Jafari, T. H. J. Vaneker, and I. Gibson, 'Wire and arc additive manufacturing: Opportunities and challenges to control the quality and accuracy of manufactured parts', *Mater Des*, vol. 202, Apr. 2021, doi: 10.1016/j.matdes.2021.109471.

[13]   V. Gornyakov, J. Ding, Y. Sun, and S. Williams, 'Understanding and designing post-build rolling for mitigation of residual stress and distortion in wire arc additively manufactured components', *Mater Des*, vol. 213, Jan. 2022, doi: 10.1016/j.matdes.2021.110335.

[14]   R. Kawalkar, H. K. Dubey, and S. P. Lokhande, 'Wire arc additive manufacturing: A brief review on advancements in addressing industrial challenges incurred with processing metallic alloys', in *Materials Today: Proceedings*, Elsevier Ltd, 2021, pp. 1971–1978. doi: 10.1016/j.matpr.2021.09.329.

[15]   L. Hagen *et al.*, 'High deposition rate wire-arc directed energy deposition of 316L and 316LSi: Process exploration and modelling', *Materials Science and Engineering: A*, vol. 880, Jul. 2023, doi: 10.1016/j.msea.2023.145044.

[16]   Y. Yang, X. Zhou, Q. Li, and C. Ayas, 'A computationally efficient thermo-mechanical model for wire arc additive manufacturing', *Addit Manuf*, vol. 46, Oct. 2021, doi: 10.1016/j.addma.2021.102090.

[17]   S. N. Ahmad *et al.*, 'Experimental validation of numerical simulation on deformation behaviour induced by wire arc additive manufacturing with feedstock SS316L on substrate S235', *International Journal of Advanced Manufacturing Technology*, vol. 119, no. 3–4, pp. 1951–1964, Mar. 2022, doi: 10.1007/s00170-021-08340-4.

[18]   M. J. Dantin, W. M. Furr, and M. W. Priddy, 'Toward a Physical Basis for a Predictive Finite Element Thermal Model of the LENS^{TM} Process Leveraging Dual-Wavelength Pyrometer Datasets', *Integr Mater Manuf Innov*, vol. 11, no. 3, pp. 407–417, Sep. 2022, doi: 10.1007/s40192-022-00271-6.

[19]   M. J. Dantin and M. W. Priddy, 'A Rate- and Temperature-Dependent Thermomechanical Internal State Variable Model of the Directed Energy Deposition Process', *J Mater Eng Perform*, vol. 33, no. 8, pp. 4051–4064, Apr. 2024, doi: 10.1007/s11665-024-09164-5.

[20]   L. Zhang and P. Michaleris, 'Investigation of Lagrangian and Eulerian finite element methods for modeling the laser forming process', *Finite Elements in Analysis and Design*, vol. 40, no. 4, pp. 383–405, Feb. 2004, doi: 10.1016/S0168-874X(03)00069-6.

[21]   MatWeb LLC, 'MatWeb: Online Materials Information Resource'. Accessed: Apr. 02, 2024. [Online]. Available: https://www.matweb.com/search/datasheet.aspx?matguid=c71186d128cd423d9c6d51106c015e8f&n=1

[22]   Z. Samad, N. M. Nor, and E. R. I. Fauzi, 'Thermo-Mechanical Simulation of Temperature Distribution and Prediction of Heat-Affected Zone Size in MIG Welding Process on Aluminium Alloy en AW 6082-T6', in *IOP Conference Series: Materials Science and Engineering*, Institute of Physics Publishing, 2019. doi: 10.1088/1757-899X/530/1/012016.

[23]   S. Schönegger, M. Moschinger, and N. Enzinger, 'Computational welding simulation of a plasma wire arc additive manufacturing process for high-strength steel', *European Journal of Materials*, vol. 4, no. 1, 2024, doi: 10.1080/26889277.2023.2297051.

[24]   J. Goldak, A. Chakravarti, and M. Bibby, 'A New Finite Element Model for Welding Heat Sources', 1984.

[25]   J. Ding *et al.*, 'Thermo-mechanical analysis of Wire and Arc Additive Layer Manufacturing process on large multi-layer parts', *Comput Mater Sci*, vol. 50, no. 12, pp. 3315–3322, Dec. 2011, doi: 10.1016/j.commatsci.2011.06.023.

[26]   D. P. Failla Jr and C. J. Nguyen, 'AMPES: Additive Manufacturing Process Event Series generator'. [Online]. Available: https://github.com/Computational-Mechanics-Materials-Lab/AMPES

[27]   M. Register and M. W. Priddy, 'Effects due to variations in thermal properties of maraging steel for finite element modeling of the WAAM process', 2022.